



strategy. This technique is additionally well-suited to be used with photorealistic, data-driven simulation engines such as *FlightMare* [17] and *FlightGoggles* [18], or SLAM and state estimation pipelines that directly produce 3D dense/mesh reconstructions of the environment, such as *Kimera* [19].

**Contributions.** In summary, our work presents the following contributions: a) We introduce a new data augmentation strategy, an extension of our previous work [6], enabling efficient and robust learning of a *sensorimotor* policy, capable to generate control actions directly from raw sensor measurements (e.g., images) instead of state estimates. Our approach is grounded in the output feedback RTMPC framework theory, unlike previous methods that rely on handcrafted heuristics, and leverages a 3D mesh of the environment to generate augmented data. b) We demonstrate our methodology in the context of *visuomotor* policy learning for an aerial robot, showing that it can track a trajectory from raw images with high robustness ( $> 90\%$  success rate) after a **single demonstration**, despite sensory noise and disturbances. c) We open-source our framework, available at <https://github.com/andretag>.

## II. RELATED WORKS

**Sensorimotor policy learning by imitating model-based experts.** Learning a sensorimotor policy by imitating the output of a model-based expert algorithm bypasses the computational cost of planning [8], control [6] and state estimation [10], with the potential of achieving increased robustness [7], [20] and reduced latency with respect to conventional autonomy pipelines. The sensory input typically employed is based on raw images [3], [12], [21] or pre-processed representations, such as feature tracks [7], depth maps [8], or intermediate layers of a CNN [22]. Vision is often complemented with proprioceptive information, such as the one provided by IMUs [7] or wheel encoders [21]. These approaches showcase the advantages of sensorimotor policy learning but do not leverage any data augmentation strategy. Consequently, they query the expert many times during the data collection phase, increasing time, number of demonstrations and computational effort to obtain the policy.

**Data augmentation for visuomotor and sensorimotor learning.** Traditional data augmentation strategies for *visuomotor* policy learning have focused on increasing a policy’s generalization ability by applying perturbations [23] or noise [24] directly in image space, without modifying the corresponding action. These methods do not directly address covariate shift issues caused by *process* uncertainties. The self-driving literature has developed a second class of visuomotor data augmentation strategies [15], [16], [25] capable of compensating covariate-shift issues. This class relies instead on first generating different views from synthetic cameras [15], [16] or data-driven simulators [25] and then computing a corresponding action via a handcrafted controller. These methods, however, rely on heuristics to establish relevant augmented views and the corresponding control action. Our work provides a more general methodology for

data augmentation and demonstrates it on a quadrotor system (higher-dimensional than the planar self-driving car models).

**Output feedback RTMPC.** Model predictive control [26] leverages a model of the system dynamics to generate actions that take into account state and actuation constraints. This is achieved by solving a constrained optimization problem along a predefined temporal horizon, using the model to predict the effects of future actions. Robust variants of MPC, such as RTMPC, usually assume that the system is subject to additive, bounded *process* uncertainty (e.g., disturbances, model errors). As a consequence, they modify nominal plans by either a) assuming a worst-case disturbance [27], [28], or b) employing an auxiliary (ancillary) controller. This controller maintains the system within some distance (“cross-section” of a tube) from the nominal plan regardless of the realization of the disturbances [29], [30]. *Output feedback* RTMPC [31]–[33] also accounts for the effects of *sensing* uncertainty (e.g., sensing noise, imperfect state estimation). Our work relies on an output feedback RTMPC [32], [33] to generate demonstrations and a data augmentation strategy. However, thanks to the proposed imitation learning strategy, our approach does not require solving the optimization problem online, reducing the onboard computational cost.

## III. PROBLEM STATEMENT

Our goal is to generate a deep neural network sensorimotor policy  $\pi_\theta$ , with parameters  $\theta$ , to control a mobile robot (e.g., multirotor). The policy needs to be capable of tracking a desired reference trajectory given high-dimensional noisy sensor measurements, and has the form

$$\mathbf{u}_t = \pi_\theta(\mathbf{o}_t, \mathbf{X}_t^{\text{des}}), \quad (1)$$

where  $t$  denotes the discrete time index,  $\mathbf{u}_t$  represents the deterministic control actions, and  $\mathbf{o}_t = (\mathcal{I}_t, \mathbf{o}_{\text{other},t})$  the high-dimensional, noisy sensor measurements, comprised of an image  $\mathcal{I}_t$  captured by an onboard camera, and other noisy measurements  $\mathbf{o}_{\text{other},t}$  (e.g., attitude, velocity). The  $N + 1$  steps of the reference trajectory are written as  $\mathbf{X}_t^{\text{des}} = \{\mathbf{x}_{0|t}^{\text{des}}, \dots, \mathbf{x}_{N|t}^{\text{des}}\}$ , where  $\mathbf{x}_{i|t}^{\text{des}}$  indicates the desired state at the future time  $t + i$ , as given at the current time  $t$ , and  $N > 0$  represents the total number of given future desired states. Our objective is to *efficiently* learn the policy parameters  $\hat{\theta}^*$  by leveraging IL and demonstrations provided by a model-based controller (*expert*).

**System model.** We assume available a model of the dynamics of the robot, described by a set of linear (e.g., via linearization), discrete and time-invariant equations:

$$\mathbf{x}_{t+1} = \mathbf{A}\mathbf{x}_t + \mathbf{B}\mathbf{u}_t + \mathbf{w}_t \quad (2)$$

where matrices  $\mathbf{A} \in \mathfrak{R}^{n_x \times n_x}$  and  $\mathbf{B} \in \mathfrak{R}^{n_x \times n_u}$  represent the system dynamics,  $\mathbf{x}_t \in \mathbb{X} \subset \mathfrak{R}^{n_x}$  represents the state of the system, and  $\mathbf{u}_t \in \mathbb{U} \subset \mathfrak{R}^{n_u}$  represents the control inputs. The system is subject to state and inputs constraint  $\mathbb{X}$  and  $\mathbb{U}$ , assumed to be convex polytopes containing the origin [31]. The quantity  $\mathbf{w}_t \in \mathbb{W} \subset \mathfrak{R}^{n_x}$  in (2) captures time-varying additive *process* uncertainties. This includes disturbances and model errors that the system may encounter

at deployment time, or the ones caused by the *sim2real* gap when collecting demonstrations using a simulator. It can additionally capture disturbances encountered at deployment time that are not present when collecting demonstrations from a real robot in a controlled environment (e.g., *lab2real* gap). These uncertainties are assumed to belong to a bounded set  $\mathbb{W}$ , assumed to be a polytope containing the origin [31].

**Sensing model.** We assume that the model describing the measurement  $\bar{\mathbf{o}}_t \in \mathfrak{R}^{n_o}$  used by the expert is:

$$\bar{\mathbf{o}}_t = \begin{bmatrix} \mathbf{o}_{\text{pos},t} \\ \mathbf{o}_{\text{other},t} \end{bmatrix} = \mathbf{C}\mathbf{x}_t + \mathbf{v}_t, \quad (3)$$

where  $\mathbf{C} \in \mathfrak{R}^{n_x \times n_o}$ , and  $\mathbf{v}_t = [\mathbf{v}_{\text{cam},t}^T, \mathbf{v}_{\text{other},t}^T]^T \in \mathbb{V} \subset \mathfrak{R}^{n_o}$  represents additive *sensing* uncertainties (e.g., noise, biases), sampled from a bounded set  $\mathbb{V}$ . The expert has access to a vision-based position estimator  $g_{\text{cam}}$  that produces a noisy estimate  $\mathbf{o}_{\text{pos}} \in \mathfrak{R}^3$  of the position  $\mathbf{p}_t \in \mathfrak{R}^3$  of the robot from an image:

$$\mathbf{o}_{\text{pos},t} = g_{\text{cam}}(\mathcal{I}_t) = \mathbf{p}_t + \mathbf{v}_{\text{cam},t}, \quad (4)$$

where  $\mathbf{v}_{\text{cam},t}$  is the associated noise/uncertainty.  $\mathbb{V}$  can be obtained via system identification, and/or prior knowledge on the accuracy of  $g_{\text{cam}}$ .

**State estimator model.** We assume that the dynamics of the state estimator employed by the expert during the demonstration collection phase can be approximated by the linear (Luenberger) observer

$$\hat{\mathbf{x}}_{t+1} = \mathbf{A}\hat{\mathbf{x}}_t + \mathbf{B}\mathbf{u}_t + \mathbf{L}(\bar{\mathbf{o}}_t - \hat{\mathbf{o}}_t), \quad \hat{\mathbf{o}}_t = \mathbf{C}\hat{\mathbf{x}}_t, \quad (5)$$

where  $\hat{\mathbf{o}}_t$  is the predicted observation, and  $\hat{\mathbf{x}}_t \in \mathfrak{R}^{n_x}$  is the estimated state.  $\mathbf{L} \in \mathbb{R}^{n_x \times n_o}$  is the observer gain matrix, and is chosen so that the matrix  $\mathbf{A} - \mathbf{L}\mathbf{C}$  is Schur stable. The observability index of the system  $(\mathbf{A}, \mathbf{C})$  is assumed to be 1, meaning that full state information can be retrieved from a single noisy measurement. In this case, the observer plays the critical role of filtering out the effects of noise and sensing uncertainties. Finally, we assume that the state estimation dynamics and noise sensitivity of the learned policy will approximately match the ones of the observer.

#### IV. METHODOLOGY

The overall idea of our method is to generate trajectory tracking demonstrations from noisy sensor measurements using an output feedback RTMPC expert combined with a state estimator (5), leveraging the defined process and sensing models. The chosen output feedback RTMPC framework is based on [33], with its cost function modified to track a desired trajectory, and it is summarized in Section IV-B. This framework provides: a) *robust* demonstrations, taking into account the effect of process *and* sensing uncertainties, and b) a corresponding data augmentation strategy, key to overcome efficiency and robustness challenges in IL. Demonstrations can be collected via IL methods such as BC [3] or DAgger [2]. Combined with the augmented data provided by our strategy, the collected demonstrations are then used to train a policy (1) via supervised regression. Section V-A will tailor our methodology to control a multirotor system.

#### A. Mathematical preliminaries

**Set operations.** Given the convex polytopes  $\mathbb{A} \subset \mathfrak{R}^n, \mathbb{B} \subset \mathfrak{R}^n$  and the linear mapping  $\mathbf{C} \in \mathfrak{R}^{m \times n}$ , we define:

- a) Minkowski sum:  $\mathbb{A} \oplus \mathbb{B} := \{\mathbf{a} + \mathbf{b} \in \mathfrak{R}^n \mid \mathbf{a} \in \mathbb{A}, \mathbf{b} \in \mathbb{B}\}$
- b) Pontryagin diff.:  $\mathbb{A} \ominus \mathbb{B} := \{\mathbf{c} \in \mathfrak{R}^n \mid \mathbf{c} + \mathbf{b} \in \mathbb{A}, \forall \mathbf{b} \in \mathbb{B}\}$

**Robust Positive Invariant (RPI) set.** Given a closed-loop Schur-stable system  $\mathbf{A} \in \mathfrak{R}^{n \times n}$  subject to the uncertainty  $\mathbf{d}_t \in \mathbb{D} \subset \mathfrak{R}^n$ :  $\boldsymbol{\xi}_{t+1} = \mathbf{A}\boldsymbol{\xi}_t + \mathbf{d}_t$ , we define the *minimal* Robust Positive Invariant (RPI) set  $\mathbb{S}$  as the *smallest* set satisfying the following property:

$$\boldsymbol{\xi}_0 \in \mathbb{S} \implies \boldsymbol{\xi}_t \in \mathbb{S}, \forall \mathbf{d}_t \in \mathbb{D}, t > 0. \quad (6)$$

This means that if the initial state  $\boldsymbol{\xi}_0$  of the system starts in the RPI set  $\mathbb{S}$ , then it will never escape from such set, regardless of the realizations  $\mathbf{d}_t$  of the disturbances in  $\mathbb{D}$ .

#### B. Output feedback robust tube MPC for trajectory tracking

The objective of the output feedback RTMPC for trajectory tracking is to regulate the system in (2) along a given *desired* trajectory  $\mathbf{X}_t^{\text{des}}$ , while ensuring satisfaction of the state and actuation constraints  $\mathbb{X}, \mathbb{U}$  regardless of the process noise  $\mathbf{w}$  and sensing noise  $\mathbf{v}$  in (2) and (3), respectively.

**Optimization problem.** To fulfill these requirements, the RTMPC computes at every timestep  $t$  a sequence of “safe” reference states  $\bar{\mathbf{X}}_t = \{\bar{\mathbf{x}}_{0|t}, \dots, \bar{\mathbf{x}}_{N|t}\}$  and actions  $\bar{\mathbf{U}}_t = \{\bar{\mathbf{u}}_{0|t}, \dots, \bar{\mathbf{u}}_{N-1|t}\}$  along a planning horizon of length  $N+1$ . This is achieved by solving the optimization problem:

$$\begin{aligned} \bar{\mathbf{U}}_t^*, \bar{\mathbf{X}}_t^* = \underset{\bar{\mathbf{U}}_t, \bar{\mathbf{X}}_t}{\text{argmin}} & \|\mathbf{e}_{N|t}\|_{\mathbf{P}}^2 + \sum_{i=0}^{N-1} \|\mathbf{e}_{i|t}\|_{\mathbf{Q}}^2 + \|\mathbf{u}_{i|t}\|_{\mathbf{R}}^2 \\ \text{subject to} & \bar{\mathbf{x}}_{i+1|t} = \mathbf{A}\bar{\mathbf{x}}_{i|t} + \mathbf{B}\bar{\mathbf{u}}_{i|t}, \\ & \bar{\mathbf{x}}_{i|t} \in \bar{\mathbb{X}}, \bar{\mathbf{u}}_{i|t} \in \bar{\mathbb{U}}, \\ & \bar{\mathbf{x}}_{N|t} \in \bar{\mathbb{X}}_N, \hat{\mathbf{x}}_t \in \mathbb{Z} \oplus \bar{\mathbf{x}}_{0|t}, \end{aligned} \quad (7)$$

where  $\mathbf{e}_{i|t} = \bar{\mathbf{x}}_{i|t} - \mathbf{x}_{i|t}^{\text{des}}$  represents the trajectory tracking error. The positive definite matrices  $\mathbf{Q}$  (size  $n_x \times n_x$ ) and  $\mathbf{R}$  (size  $n_u \times n_u$ ) are tuning parameters, and define the trade-off between deviations from the desired trajectory and actuation usage. A terminal cost  $\|\mathbf{e}_{N|t}\|_{\mathbf{P}}^2$  and terminal state constraint  $\bar{\mathbf{x}}_{N|t} \in \bar{\mathbb{X}}_N$  are introduced to ensure stability [33], where  $\mathbf{P}$  (size  $n_x \times n_x$ ) is a positive definite matrix, obtained by solving the infinite horizon optimal control LQR problem, using the system dynamics  $\mathbf{A}, \mathbf{B}$  in (2) and the weights  $\mathbf{Q}$  and  $\mathbf{R}$ . The “safe” references  $\bar{\mathbf{X}}_t, \bar{\mathbf{U}}_t$  are generated based on the nominal (e.g., not perturbed) dynamics, via the constraints  $\bar{\mathbf{x}}_{i+1|t} = \mathbf{A}\bar{\mathbf{x}}_{i|t} + \mathbf{B}\bar{\mathbf{u}}_{i|t}$ .

**Ancillary controller.** The control input for the real system is obtained via a feedback controller, called *ancillary controller*:

$$\mathbf{u}_t = \bar{\mathbf{u}}_t^* + \mathbf{K}(\hat{\mathbf{x}}_t - \bar{\mathbf{x}}_t^*), \quad (8)$$

where  $\bar{\mathbf{u}}_{0|t}^* = \bar{\mathbf{u}}_t^*$  and  $\bar{\mathbf{x}}_{0|t}^* = \bar{\mathbf{x}}_t^*$ . The matrix  $\mathbf{K}$  is computed by solving the LQR problem with  $\mathbf{A}, \mathbf{B}, \mathbf{Q}, \mathbf{R}$ . This controller ensures that the system remains inside a set  $\mathbb{Z}$  (“cross-section” of a *tube*) centered around  $\bar{\mathbf{x}}_t^*$  regardless of the realization of process and sensing uncertainty, provided that the state of the system starts in such tube (constraint  $\hat{\mathbf{x}}_t \in \mathbb{Z} \oplus \bar{\mathbf{x}}_{0|t}$ ).

**Tube and robust constraint satisfaction.** Process and sensing uncertainties are taken into account by tightening the constraints  $\mathbb{X}, \mathbb{U}$  by an amount which depends on  $\mathbb{Z}$ , obtaining  $\bar{\mathbb{X}}$  and  $\bar{\mathbb{U}}$ .

We start by describing how to compute the set  $\mathbb{Z}$ , which depends on the errors caused by uncertainties when employing the ancillary controller (8) and the state estimator (5). The system considered in (2) and (3) is subject to *sensing*  $\mathbb{V}$  and *process*  $\mathbb{W}$  uncertainties, sources of two errors: a) the state estimation error  $\xi_t^{\text{est}} = \mathbf{x}_t - \hat{\mathbf{x}}_t$ , which captures the deviations of the state estimate  $\hat{\mathbf{x}}_t$  from the true state  $\mathbf{x}_t$  of the system; b) the control error  $\xi_t^{\text{ctrl}} = \hat{\mathbf{x}}_t - \bar{\mathbf{x}}_t^*$ , which captures instead deviations of  $\hat{\mathbf{x}}_t$  from the reference plan  $\bar{\mathbf{x}}_t^* = \bar{\mathbf{x}}_{0|t}^*$ . These errors can be combined in a vector  $\xi_t = [\xi_t^{\text{est}T}, \xi_t^{\text{ctrl}T}]^T$  whose dynamics evolve according to (see [32], [33]):

$$\xi_{t+1} = \mathbf{A}_\xi \xi_t + \delta_t, \quad \delta_t \in \mathbb{D} \quad (9)$$

$$\mathbf{A}_\xi = \begin{bmatrix} \mathbf{A} - \mathbf{L}\mathbf{C} & \mathbf{0}_{n_x} \\ \mathbf{L}\mathbf{C} & \mathbf{A} + \mathbf{B}\mathbf{K} \end{bmatrix}, \quad \mathbb{D} = \begin{bmatrix} \mathbf{I}_{n_x} & -\mathbf{L} \\ \mathbf{0}_{n_x} & \mathbf{L} \end{bmatrix} \begin{bmatrix} \mathbb{W} \\ \mathbb{V} \end{bmatrix}.$$

We observe that, by design,  $\mathbf{A}_\xi$  is Schur-stable, and  $\mathbb{D}$  is a convex polytope. Then, the possible set of state estimation and control errors correspond to the minimal RPI set  $\mathbb{S}$  associated with the system  $\mathbf{A}_\xi$  under the uncertainty set  $\mathbb{D}$ .

We now introduce the error between the true state  $\mathbf{x}_t$  and the reference state  $\bar{\mathbf{x}}_t^*$ :  $\xi^{\text{tot}} = \mathbf{x}_t - \bar{\mathbf{x}}_t^* = \xi^{\text{ctrl}} + \xi^{\text{est}}$ . As a consequence, the set (*tube*)  $\mathbb{Z}$  that describes the possible deviations of the true state  $\mathbf{x}_t$  from the reference  $\bar{\mathbf{x}}_t^*$  is:

$$\mathbb{Z} = [\mathbf{I}_{n_x} \quad \mathbf{I}_{n_x}] \mathbb{S}. \quad (10)$$

Finally, the effects of noise and uncertainties can be taken into account by tightening the constraints of an amount:

$$\bar{\mathbb{X}} := \mathbb{X} \ominus \mathbb{Z}, \quad \bar{\mathbb{U}} := \mathbb{U} \ominus [\mathbf{0}_{n_x} \quad \mathbf{K}] \mathbb{S}. \quad (11)$$

### C. Tube-guided data augmentation for visuomotor learning

**Imitation learning objective.** We assume that the given output feedback RTMPC controller in (7), (8) and the state observer in (3) can be represented via a policy  $\pi_{\theta^*}$  [34], where  $\pi$  is of the form in (1), with parameters  $\theta^*$ . Our objective is to design an IL and data augmentation strategy to efficiently learn the parameters  $\hat{\theta}^*$  for the sensorimotor policy (1), collecting demonstrations from the expert. Using IL, this objective is achieved by minimizing the expected value of a distance metric  $J(\theta, \theta^* | \tau)$  over a distribution of trajectories  $\tau$ :

$$\hat{\theta}^* = \arg \min_{\theta} \mathbb{E}_{p(\tau | \pi_{\theta}, \mathcal{K}_{\text{target}})} [J(\theta, \theta^* | \tau)], \quad (12)$$

where  $J(\theta, \theta^* | \tau)$  captures the differences between the trajectories generated by the expert  $\pi_{\theta^*}$  and the trajectories produced by the learner  $\pi_{\theta}$ . The variable  $\tau := ((\mathbf{o}_0, \mathbf{u}_0, \mathbf{X}_0^{\text{des}}), \dots, (\mathbf{o}_T, \mathbf{u}_T, \mathbf{X}_T^{\text{des}}))$  denotes a  $T + 1$  step (observation, action, reference) trajectory sampled from the distribution  $p(\tau | \pi_{\theta}, \mathcal{K}_{\text{target}})$ . Such distribution represents all the possible trajectories induced by the learner policy  $\pi_{\theta}$  in the deployment environment  $\mathcal{K}_{\text{target}}$ , under all the possible

instances of the process *and* sensing uncertainties. In this work, the chosen distance metric is the MSE loss:

$$J(\theta, \theta^* | \tau) = \frac{1}{T} \sum_{t=0}^{T-1} \|\pi_{\theta}(\mathbf{o}_t, \mathbf{X}_t^{\text{des}}) - \pi_{\theta^*}(\mathbf{o}_t, \mathbf{X}_t^{\text{des}})\|_2^2. \quad (13)$$

As observed in [6], the presence of uncertainties in the deployment domain  $\mathcal{K}_{\text{target}}$  makes the setup challenging, as demonstrations are usually collected in a training environment  $\mathcal{K}_{\text{source}}$  that presents only a subset of all the possible uncertainty realizations. At deployment time, uncertainties may drive the learned policy towards the region of the input space for which no demonstrations have been provided (covariate shift), with potentially catastrophic consequences.

**Tube and ancillary controller for data augmentation.** To overcome these limitations, we design a data augmentation strategy that takes into account and compensates for the effects of *process and sensing uncertainties* encountered in  $\mathcal{K}_{\text{target}}$ , and that it is capable of producing the augmented input-output data needed to learn the sensorimotor policy (1). We do so by extending our previous approach [6], named Sampling Augmentation (SA), which provides a strategy to efficiently learn a policy robust to *process* uncertainty. SA relies on recognizing that the tube  $\mathbb{Z}$ , as computed via a RTMPC, represents a model of the states that the system may visit when subject to process uncertainties. The ancillary controller (8) provides a computationally efficient way to generate the actions to take inside the tube, as it guarantees that the system remains inside the tube for every possible realization of the process uncertainty.

Our new approach, named Visuomotor Sampling Augmentation (VSA), employs the output feedback variant of RTMPC in Section IV-B, as its tube represents a model of the states that might be visited by the system when subject to process *and sensing* uncertainty, and its ancillary controller provides a way to efficiently compute corresponding actions, guaranteeing that the system remains inside the tube  $\mathbb{Z} \oplus \bar{\mathbf{x}}_t^*$  in (10) for every possible realization of  $\mathbf{w}_t \in \mathbb{W}$  and  $\mathbf{v}_t \in \mathbb{V}$ . These properties can be leveraged to design a data augmentation strategy while collecting demonstrations in the source domain  $\mathcal{K}_{\text{source}}$ .

More specifically, let  $\tau^{\text{aux}}$  be a  $T + 1$  step demonstration generated by the output feedback RTMPC in Section IV-B, collected in the training domain  $\mathcal{K}_{\text{source}}$ :

$$\tau^{\text{aux}} = ((\mathbf{o}_0, \mathbf{u}_0, (\bar{\mathbf{u}}_0^*, \bar{\mathbf{x}}_0^*), \mathbf{X}_0^{\text{des}}), \dots, (\mathbf{o}_T, \mathbf{u}_T, (\bar{\mathbf{u}}_T^*, \bar{\mathbf{x}}_T^*), \mathbf{X}_T^{\text{des}})). \quad (14)$$

Then, at every timestep  $t$  in the collected demonstration  $\tau^{\text{aux}}$ , we can compute extra (state, action) pairs  $(\mathbf{x}^+, \mathbf{u}^+)$  by sampling extra states from inside the tube  $\mathbf{x}^+ \in \bar{\mathbf{x}}_t^* \oplus \mathbb{Z}$ , and the corresponding robust control action  $\mathbf{u}^+$ :

$$\mathbf{u}^+ = \bar{\mathbf{u}}_t^* + \mathbf{K}(\mathbf{x}^+ - \bar{\mathbf{x}}_t^*). \quad (15)$$

**Augmented sensory data generation.** The output feedback RTMPC-based augmentation strategy described so far provides a way to generate extra (state, action) samples for data augmentation, but not the sensor observations  $\mathbf{o}^+ =$

$(\mathcal{I}^+, \mathbf{o}_{\text{other}}^+)$  required as input of the sensorimotor policy (1). We overcome this issue by employing observation models (3) available for the expert, obtaining a way to generate extra observations  $\mathbf{o}^+$ , given extra states  $\mathbf{x}^+$ .

In the context of learning the visuomotor policy (1), we generate synthetic camera images  $\mathcal{I}^+$  via an inverse pose estimator  $g_{\text{cam}}^{-1}$ , mapping camera poses  $\mathbf{T}_{IC}$  to image observations  $\mathcal{I}$

$$\mathcal{I}^+ = g_{\text{cam}}^{-1}(\mathbf{T}_{IC}^+) \quad (16)$$

where  $\mathbf{T}_{IC}$  denotes a homogeneous transformation matrix [35] from a world (inertial) frame  $I$  to a camera frame  $C$ . The inverse camera model  $g_{\text{cam}}^{-1}$  can be obtained by generating a 3D reconstruction of the environment from the sequence of observations obtained in the collected demonstrations, and by modeling the intrinsic and extrinsic parameters of the onboard camera used by the robot [35]. Extra camera poses  $\mathbf{T}_{IC}^+$  can be obtained from the extra state vector  $\mathbf{x}^+$ , assuming that the state contains position and orientation information

$$\mathbf{T}_{IC}^+ = \mathbf{T}_{IB}(\mathbf{x}^+) \mathbf{T}_{BC}, \quad (17)$$

where  $\mathbf{T}_{IB}$  represents the homogeneous transformation expressing the pose of a robot-fixed body frame  $B$  with respect to  $I$ .  $\mathbf{T}_{BC}$  describes a known rigid transformation between the body of the robot  $B$  and the optical frame of the camera  $C$ . The full extra observation  $\mathbf{o}^+$  can be obtained by additionally computing  $\mathbf{o}_{\text{other}}^+$  via the measurement model (3), assuming zero noise:

$$\mathbf{o}^+ = (\mathcal{I}^+, \mathbf{o}_{\text{other}}^+), \quad \mathbf{o}_{\text{other}}^+ = \mathbf{S} \mathbf{C} \mathbf{x}^+, \quad (18)$$

where  $\mathbf{S}$  is a selection matrix.

## V. EVALUATION

### A. Visuomotor trajectory tracking on a multirotor

**Task setup.** We consider the task of learning a visuomotor trajectory tracking policy for a multirotor, starting from slightly different initial states. The chosen trajectory is an eight-shape (lemniscate), with a velocity of up to 3.5 m/s and a total duration of 30.0 s. We assume that the robot is equipped with a downward-facing monocular camera, and it has available onboard noisy velocity  ${}_I \mathbf{v} \in \mathfrak{R}^3$  and roll  ${}_I \varphi$ , pitch  ${}_I \vartheta$  information, corrupted by measurement noise  $\mathbf{v}_{\text{other},t}$ :

$$\mathbf{o}_{\text{other},t} = [{}_I \mathbf{v}^T, {}_I \varphi, {}_I \vartheta]^T + \mathbf{v}_{\text{other},t}. \quad (19)$$

$I$  denotes a yaw-fixed, gravity aligned inertial reference frame in which the quantities are expressed, and  $\mathbf{v}_{\text{other}}$  is a zero-mean, Gaussian noise with three standard deviations  $3\sigma_{\text{other}} = [0.2, 0.2, 0.2, 0.05, 0.05]^T$  (units in  $m/s$  for velocity, and  $rad$  for tilt). Information on the position  ${}_I \mathbf{p} \in \mathfrak{R}^3$  of the robot is not provided to the learned policy, and it must be inferred from the onboard camera. The output feedback RTMPC has instead additionally access to noisy position information corrupted by additive, zero mean Gaussian noise  $\mathbf{v}_{\text{cam}}$  with three standard deviations  $3\sigma_{\text{cam}} = [0.2, 0.2, 0.4]^T$  ( $m$ ). Demonstrations are collected from the output feedback RTMPC expert in a nominal domain  $\mathcal{K}_{\text{source}}$  that presents sensing noise and model

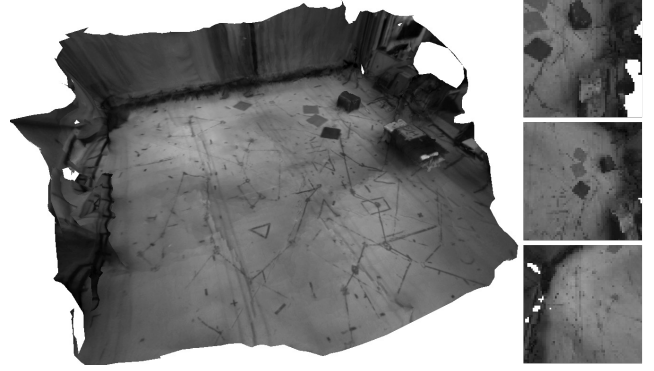


Fig. 2: *Left*: 3D reconstruction of the training environment employed to generate data augmentation. The camera images used to generate the reconstruction are obtained from a single demonstration collected with the real robot. *Right*: Images generated by the simulated onboard camera along the considered trajectory in the 3D mesh of the environment. If the camera is pointing at regions where the reconstruction is not available (e.g., top and bottom right images), the area of missing data is left *featureless* (white), without providing any additional information useful for position estimation.

uncertainties (e.g., due to drag, unmodeled attitude dynamics). We consider two deployment environments  $\mathcal{K}_{\text{target}}$ , one with sensing noise, matching  $\mathcal{K}_{\text{source}}$ , and one that additionally presents wind-like force disturbances  $\mathbf{f}_{\text{wind}}$ , with magnitude corresponding to 15%-20% of the weight of the multirotor (12.75 N). During training and deployment, the robot should not collide with the walls/ceiling nor violate additional safety limits (maximum velocity, roll, pitch).

**Output feedback RTMPC design.** To design the output feedback RTMPC, we employ a hover-linearized model of a multirotor [36]. The state of the robot ( $n_x = 8$ ) is:

$$\mathbf{x} = [{}_I \mathbf{p}^T, {}_I \mathbf{v}^T, {}_I \varphi, {}_I \vartheta]^T, \quad (20)$$

while the output ( $n_u = 3$ )  $\mathbf{u}_t$  corresponds to roll, pitch and thrust commands, which a cascaded attitude controller executes. Safety limits and position limits are encoded as state constraints. The sampling period for the controller and prediction model is set to  $T_s = 0.1$  s, and the prediction horizon is  $N = 30$ , (3.0 s). The tube  $\mathbb{Z}$  is computed assuming the observation model in (3) to be:  $\bar{\mathbf{o}}_t = \mathbf{x}_t + \mathbf{v}_t$ , where the bounded measurement uncertainty matches the three standard deviations of the noise encountered in the environment:  $\mathbb{V} = \{\mathbf{v} \mid \|\mathbf{v}\|_\infty \leq 3[\sigma_{\text{cam}}^T, \sigma_{\text{other}}^T]^T\}$ . The observer gain matrix  $\mathbf{L}$  is computed by assuming fast state estimation dynamics, by placing the poles of the estimation error dynamics  $\mathbf{A} - \mathbf{L} \mathbf{C}$  at 30.0 rad/s. The process uncertainty  $\mathbb{W}$  is set to correspond to a bounded force-like disturbance of magnitude equal to 25% of the weight of the multirotor, capturing the physical limits of the platform. Using these priors on uncertainties, sensing noise and the system (9), we compute an approximation of the tube  $\mathbb{Z}$  via Monte Carlo simulations, randomly sampling instances of the uncertainties. The RPI set  $\mathbb{S}$  is obtained by computing an axis-aligned bounding box approximation of the error trajectories.

**Policy architecture.** The architecture of the learned policy (1) is represented in Figure 3. The policy takes as input the raw image produced by the onboard camera, the desired trajectory, and noisy attitude and velocity information  $\mathbf{o}_{\text{other}}$ . It employs three convolutional layers, which map the raw images into a lower-dimensional feature space; these features

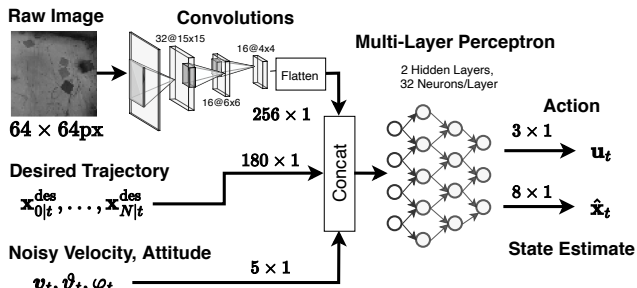


Fig. 3: Architecture of the employed visuomotor policy. The policy takes as input a raw camera image, a desired trajectory  $\mathbf{x}_{0|t}^{\text{des}}, \dots, \mathbf{x}_{N|t}^{\text{des}}$  and noisy measurements of the velocity  $\mathbf{v}_t$  and tilt (roll  $\varphi_t$ , pitch  $\vartheta_t$ ) of the multirotor. It outputs an action  $\mathbf{u}_t$ , representing a desired roll, pitch and thrust set-points for the cascaded attitude controller. The policy additionally outputs an estimate of the state  $\hat{\mathbf{x}}_t$ , which was found useful to promote learning of features relevant for position estimation.

are then combined with the additional velocity and attitude inputs, and passed through a series of fully connected layers. The generated action  $\mathbf{u}_t$  is then clipped such that  $\mathbf{u}_t \in \mathcal{U}$ . To promote learning of internal features relevant to estimating the robot’s state, the output of the policy is augmented to predict the current state  $\hat{\mathbf{x}}$  (or  $\mathbf{x}^+$  for the augmented data), modifying (13) accordingly. This output is not used at deployment time, but it was found to improve the performance.

### B. Dense reconstruction of the environment

We generate a 3D mesh of the environment needed for data augmentation via VSA from a sequence of real images collected by the onboard downward-facing camera of the Qualcomm Snapdragon Flight Pro [37] board mounted on a multirotor. The images are obtained by executing the trajectory that we intend to learn, which helps us validate the assumption that it is possible to collect a quantity and quality of images sufficient to create an accurate 3D mesh from a single demonstration. Overall we employ 145 black and white images of size  $640 \times 480$  pixels. The 3D reconstruction of the considered indoor flight space and the resulting mesh, shown in Figure 2 (left), are generated via the 3D photogrammetry pipeline provided by *Meshroom* [38]. The scale of the generated reconstruction, which is unobservable from the monocular images, is set manually via prior knowledge of the dimensions of the environment. The obtained mesh is then integrated with our multirotor simulator. We additionally simulate a pinhole camera, whose extrinsic and intrinsic are set to approximately match the parameters of the real onboard camera. Figure 2 (right) shows examples of synthetic images from our simulator.

### C. Choice of baselines, training setup and hyperparameters

Demonstration collection, training and evaluation is performed in simulation, employing a realistic full nonlinear multirotor model (e.g., [36]). We apply our data augmentation strategy, VSA, to BC and DAgger, comparing their performance without any data augmentation. We additionally combine BC and DAgger with Domain Randomization (DR); in this case, during demonstration collection, we apply wind disturbances with magnitude sampled from 10%-110% of the maximum wind force at deployment. We set  $\beta$ , hyperparameter of DAgger controlling the probability of

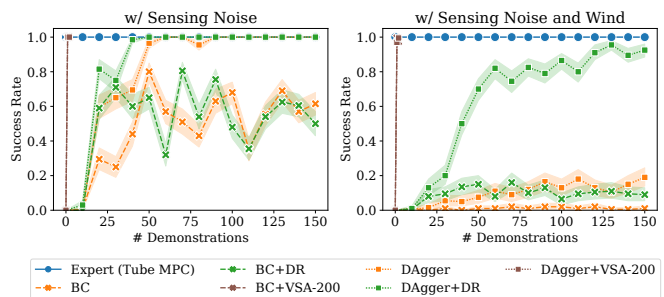


Fig. 4: Robustness in the deployment domains under measurement uncertainties (sensing noise) and process noise (wind-like disturbances) as a function of the number of demonstrations. The shaded area represent the 95% confidence intervals. Our approach, Visuomotor Sampling Augmentation (VSA)-200 (where 200 indicates the number of samples extracted from the tube per timestep), after a single demonstration achieves full robustness in the environment w/o wind, and  $> 95\%$  robustness in the environment with wind. Evaluation performed across 10 random seeds, with 20 trajectories per seed, starting from different initial states. The lines of the VSA-based approaches overlap.

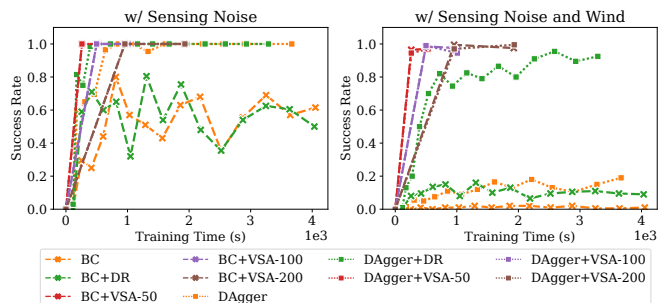


Fig. 5: Robustness as a function of the training time, which includes the time to collect demonstrations from the expert and to train the policy. Robustness is considered under only measurement uncertainties (sensing noise) and in combination with process noise (wind-like disturbances). This result highlights that our approach, Visuomotor Sampling Augmentation (VSA), is capable to achieve  $> 95\%$  robustness under sensing and process noise in less than half of the time than the best performing baseline approaches (DAgger+DR). Reducing the number of samples extracted from the tube (VSA-{50, 100, 200}) significantly reduces the training time, with a minimal change in robustness.

using actions from the expert instead of the learner policy, to be  $\beta = 1$  for the first set of demonstrations, and  $\beta = 0$  otherwise. For every method, we perform our analysis in  $M$  iterations, where at every  $m$ th iteration we: (i) collect  $K$  new demonstrations via the output feedback RTMPC expert and the state estimator; (ii) train a policy with randomly initialized weights using all the demonstrations collected so far, and (iii) evaluate the obtained policy for 20 times, under different realizations of the uncertainty and initial states of the robot. We record the time taken to perform phase (i)-(ii) at the  $m$ th iteration, denoted as  $T_m^{\text{iter}}$ . The entire analysis is repeated across 10 random seeds. We use  $M = 2$ ,  $K = 1$  for methods using VSA, while  $M = 15$ ,  $K = 10$  for all the other methods, in order to speed up their computation. When using VSA, we additionally train the policy incrementally, i.e., we only use the newly collected demonstrations and the corresponding augmented data to update the previously trained policy. All the policies are trained for 50 epochs using the ADAM optimizer, with a learning rate of 0.001 and a batch size of 32. When using VSA, we augment the training data by generating a number  $S = \{50, 100, 200\}$  of observation-action samples, for every timestep, by uniformly sampling states inside the tube. We denote the corresponding method as VSA- $S$ .

TABLE I: Properties of the considered visuomotor policy learning approaches, including robustness, performance, and demonstration efficiency. We define an approach *easy* if it does not require applying disturbances during the demonstration collection phase, and it is *safe* if it does not violate state constraints (e.g., wall collision) during training. *Performance* captures the relative error between the trajectory generated by output feedback RTMPC (expert) and the learned policy. *Demonstration efficiency* indicates the number of demonstrations required for one approach to achieve at least 90% *success rate*. Performance and robustness of the baseline approaches are evaluated after 150 demonstrations, while VSA methods are evaluated after *only* 2 demonstrations.

Method	Training		Robustness		Performance		Demonstration			
	Robustif.	Imitation	Easy	Safe	succ. rate (% , $\uparrow$ )	expert gap (% , $\downarrow$ )	Efficiency ( $\downarrow$ )	Noise, Wind		
BC			Yes	Yes	59.3	0.8	98.4	545.7	-	-
DAgger			Yes	No	100.0	17.0	8.3	295.2	50	-
DR			No	Yes	55.3	9.3	128.0	186.7	-	-
DAgger			No	No	100.0	91.0	5.4	27.3	40	120
VSA-50			Yes	Yes	100.0	97.0	27.4	24.3	1	1
DAgger			Yes	Yes	100.0	97.0	13.6	17.5	1	1
VSA-100			Yes	Yes	100.0	97.5	11.5	14.1	1	1
DAgger			Yes	Yes	100.0	94.5	8.9	13.0	1	1
VSA-200			Yes	Yes	100.0	97.5	12.7	17.9	1	1
DAgger			Yes	Yes	100.0	99.5	4.5	14.9	1	1

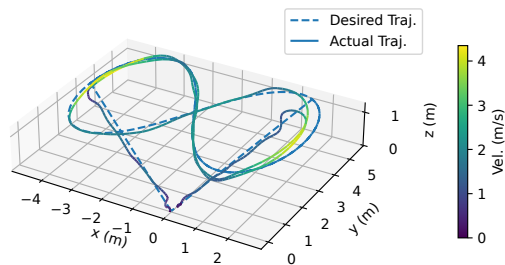
TABLE II: Trajectory tracking errors. The position error is expressed in  $m^2$ , while velocity error in  $m^2/s^2$ .

		DAgger+VSA-100		Expert	
		Noise	Noise, Wind	Noise	Noise, Wind
MSE	Pos.	0.332	0.593	0.256	0.562
	Vel.	0.579	0.626	0.563	0.598

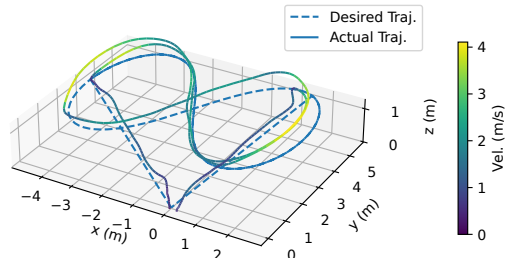
#### D. Efficiency, robustness and performance

**Robustness and efficiency.** We evaluate the robustness of the considered methods by monitoring the *success rate*, as the percentage of episodes where the robot never violates any state constraint in the considered deployment environment. This metric is evaluated as a function of the number of demonstrations collected in the source environment. The results are shown in Figure 4 and Table I, and highlight that all VSA methods, combined with either DAgger or BC, can achieve complete robustness in the environment without wind after a single demonstration, and at least 94.5% success rate in the environment with wind (DAgger+VSA-50). A second demonstration can provide  $> 99\%$  robustness even in the environment with wind (DAgger+VSA-200). The baseline approaches require instead 40-50 demonstrations to achieve full success rate in the environment without wind, and the best performing baseline (DAgger+DR) requires 120 demonstrations to achieve its top robustness (97.3% success rate) in the more challenging environment. We additionally evaluate the computational efficiency as the time (*training time*) required to achieve a certain success rate. This is done by monitoring the robustness achieved at the  $m$ th iteration as a function of the time to reach that iteration,  $\sum_{i=0}^m T_i^{\text{iter}}$ . The results in Figure 5 highlight that our approach requires less than *half* training time than the best performing baseline (DAgger+DR) to achieve higher or comparable robustness in the most challenging environment. Additionally, reducing the number of samples in VSA can enable large training time gains with a minimal loss in robustness.

**Performance at convergence.** We evaluate the performance of the considered approaches via the *expert gap*, capturing the relative error with respect to the output feedback RTMPC expert of the stage cost  $\sum_t \|e_t\|_Q^2 + \|u_t\|_R^2$  along the trajectories executed in the two considered deployment environment. We exclude from the performance evaluation



(a) With sensing noise, no wind.



(b) With sensing noise and wind gusts.

Fig. 6: Executed trajectory and velocity of the multicopter in our simulated environment under sensing noise and challenging wind-like disturbances. The policy has been trained from a *single* demonstration using DAgger+VSA-100. The wind disturbances applied are force steps, representing wind gusts, ranging 15% to 20% of the weight of the robot, and varying in magnitude and direction every 4.0 s.

TABLE III: Computation time required to generate a new action for the output feedback RTMPC (Expert) and the proposed learned visuomotor neural network policy (Policy), given a sensory observation. The learned neural network policy is 17.6 times faster than the optimization-based expert.

		Time (ms)			
Method	Setup	Mean	St. Dev.	Min	Max
Expert	CVXPY [39]	15.70	13.37	7.37	76.56
<b>Policy</b>	PyTorch	<b>0.89</b>	<b>0.03</b>	<b>0.84</b>	<b>1.02</b>

those trajectories that violate state constraints (not robust). Table I reports the *expert gap* at the convergence of the various methods. It highlights that DAgger combined with VSA (DAgger+VSA) performs comparably or better than the most robust baseline (DAgger+DR) but at a fraction of the number of demonstrations (2 instead of 150) and training time. Figure 6 shows a qualitative evaluation of the trajectory tracked by the learned policy and highlights that the robot remains close to the reference despite the relatively high velocity, wind, and sensing noise. Table II gives the corresponding MSE for the position and velocity, showing that the obtained visuomotor policy has tracking errors comparable to those of the output feedback RTMPC expert, despite using vision information to infer the position of the robot, while the expert has access to noisy ground truth position information. **Efficiency at deployment.** Table III reports the time to compute a new action. It shows that on average the compressed policy is 17.6 times faster, even when excluding the cost of state estimation, than the corresponding model-based controller. Evaluation performed on an Intel i9-10920 (12 cores) with two Nvidia RTX 3090 GPUs.

## VI. CONCLUSIONS

We have presented a strategy for efficient and robust sensorimotor policy learning. Our key idea relies on the co-design of controller and data augmentation strategy with IL methods. Such controller and data augmentation approach leverage the theory of output feedback RTMPC to compute

relevant observations and actions for data augmentation—considering the effects of sensing noise, domain uncertainties, and disturbances. We have tailored our approach to the context of visuomotor policy learning, relying on a mesh of the considered environment to generate tube-guided augmented views. Our numerical evaluation has shown that the proposed method can learn a robust visuomotor policy from a few demonstrations, outperforming IL baselines in demonstration and computational efficiency. Future works will focus on robustifying the policy to uncertainties/imperfections in the 3D mesh of the environment ( $g_{\text{cam}}^{-1}$ ), accounting for state estimation dynamics in the data augmentation procedure, and performing hardware experiments.

## ACKNOWLEDGMENT

This work was funded by the Air Force Office of Scientific Research MURI FA9550-19-1-0386.

## REFERENCES

- [1] B. D. Argall, S. Chernova, M. Veloso, and B. Browning, “A survey of robot learning from demonstration,” *Robotics and autonomous systems*, vol. 57, no. 5, pp. 469–483, 2009.
- [2] S. Ross, G. Gordon, and D. Bagnell, “A reduction of imitation learning and structured prediction to no-regret online learning,” in *Proceedings of the fourteenth international conference on artificial intelligence and statistics*. JMLR Workshop and Conference Proceedings, 2011, pp. 627–635.
- [3] D. A. Pomerleau, “Alvinn: An autonomous land vehicle in a neural network,” Carnegie-Mellon Univ Pittsburgh PA Artificial Intelligence and Psychology, Tech. Rep., 1989.
- [4] D. Scaramuzza and F. Fraundorfer, “Visual odometry [tutorial],” *IEEE Robotics Automation Magazine*, vol. 18, no. 4, pp. 80–92, 2011.
- [5] J. Zhang and S. Singh, “Loam: Lidar odometry and mapping in real-time,” in *Robotics: Science and Systems*, vol. 2, no. 9. Berkeley, CA, 2014, pp. 1–9.
- [6] A. Tagliabue, D.-K. Kim, M. Everett, and J. P. How, “Demonstration-efficient guided policy search via imitation of robust tube mpc,” in *2022 International Conference on Robotics and Automation (ICRA)*, 2022, pp. 462–468.
- [7] A. Loquercio, E. Kaufmann, R. Ranftl, A. Dosovitskiy, V. Koltun, and D. Scaramuzza, “Deep drone racing: From simulation to reality with domain randomization,” *IEEE Transactions on Robotics*, vol. 36, no. 1, pp. 1–14, 2019.
- [8] A. Loquercio, E. Kaufmann, R. Ranftl, M. Müller, V. Koltun, and D. Scaramuzza, “Learning high-speed flight in the wild,” *Science Robotics*, vol. 6, no. 59, p. eabg5810, 2021.
- [9] T. Zhang, G. Kahn, S. Levine, and P. Abbeel, “Learning deep control policies for autonomous aerial vehicles with mpc-guided policy search,” in *2016 IEEE international conference on robotics and automation (ICRA)*. IEEE, 2016, pp. 528–535.
- [10] G. Kahn, T. Zhang, S. Levine, and P. Abbeel, “Plato: Policy learning using adaptive trajectory optimization,” in *2017 IEEE International Conference on Robotics and Automation (ICRA)*. IEEE, 2017, pp. 3342–3349.
- [11] E. Kaufmann, A. Loquercio, R. Ranftl, M. Müller, V. Koltun, and D. Scaramuzza, “Deep drone acrobatics,” *arXiv preprint arXiv:2006.05768*, 2020.
- [12] S. Ross, N. Melik-Barkhudarov, K. S. Shankar, A. Wendel, D. Dey, J. A. Bagnell, and M. Hebert, “Learning monocular reactive uav control in cluttered natural environments,” in *2013 IEEE international conference on robotics and automation*. IEEE, 2013, pp. 1765–1772.
- [13] Y. Pan, C.-A. Cheng, K. Saigol, K. Lee, X. Yan, E. A. Theodorou, and B. Boots, “Imitation learning for agile autonomous driving,” *The International Journal of Robotics Research*, vol. 39, no. 2-3, pp. 286–302, 2020.
- [14] X. B. Peng, M. Andrychowicz, W. Zaremba, and P. Abbeel, “Sim-to-real transfer of robotic control with dynamics randomization,” in *2018 IEEE international conference on robotics and automation (ICRA)*. IEEE, 2018, pp. 3803–3810.
- [15] M. Bojarski, D. Del Testa, D. Dworakowski, B. Firner, B. Flepp, P. Goyal, L. D. Jackel, M. Monfort, U. Muller, J. Zhang *et al.*, “End to end learning for self-driving cars,” *arXiv preprint arXiv:1604.07316*, 2016.
- [16] A. Giusti, J. Guzzi, D. C. Cireşan, F.-L. He, J. P. Rodríguez, F. Fontana, M. Faessler, C. Forster, J. Schmidhuber, G. Di Caro *et al.*, “A machine learning approach to visual perception of forest trails for mobile robots,” *IEEE Robotics and Automation Letters*, vol. 1, no. 2, pp. 661–667, 2015.
- [17] Y. Song, S. Naji, E. Kaufmann, A. Loquercio, and D. Scaramuzza, “Flightmare: A flexible quadrotor simulator,” *arXiv preprint arXiv:2009.00563*, 2020.
- [18] W. Guerra, E. Tal, V. Murali, G. Ryou, and S. Karaman, “Flightgoggles: A modular framework for photorealistic camera, exteroceptive sensor, and dynamics simulation,” *arXiv preprint arXiv:1905.11377*, 2019.
- [19] A. Rosinol, M. Abate, Y. Chang, and L. Carlone, “Kimera: an open-source library for real-time metric-semantic localization and mapping,” in *2020 IEEE International Conference on Robotics and Automation (ICRA)*. IEEE, 2020, pp. 1689–1696.
- [20] C. Dawson, B. Lowenkamp, D. Goff, and C. Fan, “Learning safe, generalizable perception-based hybrid control with certificates,” *IEEE Robotics and Automation Letters*, vol. 7, no. 2, pp. 1904–1911, 2022.
- [21] Y. Pan, C.-A. Cheng, K. Saigol, K. Lee, X. Yan, E. Theodorou, and B. Boots, “Agile autonomous driving using end-to-end deep imitation learning,” *arXiv preprint arXiv:1709.07174*, 2017.
- [22] K. Lee, B. Vlahov, J. Gibson, J. M. Reh, and E. A. Theodorou, “Approximate inverse reinforcement learning from vision-based imitation learning,” in *2021 IEEE International Conference on Robotics and Automation (ICRA)*, 2021, pp. 10 793–10 799.
- [23] D. Hendrycks, N. Mu, E. D. Cubuk, B. Zoph, J. Gilmer, and B. Lakshminarayanan, “Augmix: A simple data processing method to improve robustness and uncertainty,” *arXiv preprint arXiv:1912.02781*, 2019.
- [24] D. Antotsiou, C. Ciliberto, and T.-K. Kim, “Adversarial imitation learning with trajectorial augmentation and correction,” *arXiv preprint arXiv:2103.13887*, 2021.
- [25] A. Amini, I. Gilitschenski, J. Phillips, J. Moseyko, R. Banerjee, S. Karaman, and D. Rus, “Learning robust control policies for end-to-end autonomous driving from data-driven simulation,” *IEEE Robotics and Automation Letters*, vol. 5, no. 2, pp. 1143–1150, 2020.
- [26] F. Borrelli, A. Bemporad, and M. Morari, *Predictive control for linear and hybrid systems*. Cambridge University Press, 2017.
- [27] P. O. Scokaert and D. Q. Mayne, “Min-max feedback model predictive control for constrained linear systems,” *IEEE Transactions on Automatic Control*, vol. 43, no. 8, pp. 1136–1142, 1998.
- [28] A. Bemporad, F. Borrelli, and M. Morari, “Min-max control of constrained uncertain discrete-time linear systems,” *IEEE Transactions on automatic control*, vol. 48, no. 9, pp. 1600–1606, 2003.
- [29] D. Q. Mayne, M. M. Seron, and S. Raković, “Robust model predictive control of constrained linear systems with bounded disturbances,” *Automatica*, vol. 41, no. 2, pp. 219–224, 2005.
- [30] B. T. Lopez, “Adaptive robust model predictive control for nonlinear systems,” Ph.D. dissertation, Massachusetts Institute of Technology, 2019.
- [31] D. Q. Mayne, S. V. Raković, R. Findeisen, and F. Allgöwer, “Robust output feedback model predictive control of constrained linear systems,” *Automatica*, vol. 42, no. 7, pp. 1217–1222, 2006.
- [32] M. Kögel and R. Findeisen, “Robust output feedback mpc for uncertain linear systems with reduced conservatism,” *IFAC-PapersOnLine*, vol. 50, no. 1, pp. 10 685–10 690, 2017.
- [33] J. Lorenzetti and M. Pavone, “A simple and efficient tube-based robust output feedback model predictive control scheme,” in *2020 European Control Conference (ECC)*. IEEE, 2020, pp. 1775–1782.
- [34] M. Laskey, J. Lee, R. Fox, A. Dragan, and K. Goldberg, “Dart: Noise injection for robust imitation learning,” in *Conference on robot learning*. PMLR, 2017, pp. 143–156.
- [35] T. D. Barfoot, *State estimation for robotics*. Cambridge University Press, 2017.
- [36] M. Kamel, M. Burri, and R. Siegwart, “Linear vs nonlinear mpc for trajectory tracking applied to rotary wing micro aerial vehicles,” *IFAC-PapersOnLine*, vol. 50, no. 1, pp. 3463–3469, 2017.
- [37] “Qualcomm Flight Pro,” Feb 2022, [Online; accessed 21. Feb. 2022]. [Online]. Available: <https://developer.qualcomm.com/hardware/qualcomm-flight-pro>



- [38] C. Griwodz, S. Gasparini, L. Calvet, P. Gurdjos, F. Castan, B. Maujean, G. De Lillo, and Y. Lanthony, "Alicevision meshroom: An open-source 3d reconstruction pipeline," in *Proceedings of the 12th ACM Multimedia Systems Conference*, 2021, pp. 241–247.
- [39] A. Agrawal, R. Verschueren, S. Diamond, and S. Boyd, "A rewriting system for convex optimization problems," *Journal of Control and Decision*, vol. 5, no. 1, pp. 42–60, 2018.